Optimization for High-Frequency Power Transformers with Multi-Winding Current Ballasting

Kishalay Datta Yue Wu Charles R. Sullivan Jason T. Stauth
Thayer School of Engineering at Dartmouth
Hanover, NH 03755 USA
Email: {Kishalay.Datta.Th, Yue.Wu.Th, Charles.R.Sullivan, Jason.T.Stauth}@dartmouth.edu

***Abstract*—This work explores optimization of multi-winding transformers which may be used for high-frequency isolated power conversion and wireless power transfer. We extend the concept of current ballasting previously used to reduce AC losses in multi-winding inductors, allowing efficient operation at higher frequencies. An analytical framework based on a multi-port impedance matrix is used to determine the optimal current for each winding that maximizes overall power transfer efficiency. Design insights for planar spiral transformers include that the optimal current distribution depends on both loss and coupling of each winding but interestingly, the relative loss fraction of each winding should be the same. The analytical model has been verified with numerical optimization and experimental measurements using wire-wound multi-winding transformer.**

I. Introduction

Galvanically isolated power conversion is critical in a number of applications where different voltage domains are stacked or floating, where rejection of common-mode noise transients is required, or where voltages are high enough to present safety challenges [1]. Even though signal isolation has been achieved by a variety of techniques, isolated power transfer predominantly uses transformers [1]–[3]. With ever increasing needs for high power density, miniaturization of such power transformers is necessary. This leads to very high-frequency (VHF) operation in the range of 30 to 300 MHz where primarily air-core transformers are practical [4]. Unfortunately, eddy currents and circulating current increase the AC resistance and hence pose a major challenge for such designs [4], [5]. For non-isolated VHF power conversion, multi-winding current ballasting techniques have been used to counter VHF circulating currents, which leads to enhanced efficiencies [6]–[8]. This has provided the key motivation for this work *i.e.,* understanding the multi-winding current ballasting concept in the context of VHF transformers.

Fig. 1 illustrates different design scenarios for planar-spiral air-core transformers, where here we refer to the conductors as traces. In examples with high current, windings may be formed with wide traces to reduce series resistance. Unfortunately, the benefit of low dc resistance using wide traces is reduced at high frequency due to skin- and proximity-effect current crowding, which reduces efficiency. In other examples where higher numbers of turns are used to support higher voltage and lower current, thinner traces may be used. While thin traces may help mitigate skin-effect current crowding, the main limitation of this approach is that, depending on the geometry of the transformer, such a uniform current distribution is sub-optimal. Intuitively, we do not want the same current in small-radius turns (closer to center of the spiral, which have low resistance) as in the turns with larger radius (outer turns of the spiral, which have higher resistance). What is even more interesting for a transformer is the dependence on the primary to secondary coupling for turns in different locations. If turns in certain locations have poor coupling compared to others, there would be no reason to force the same current without any substantial power being transmitted while still incurring substantial conduction losses. This is the foundational motivation for this work.

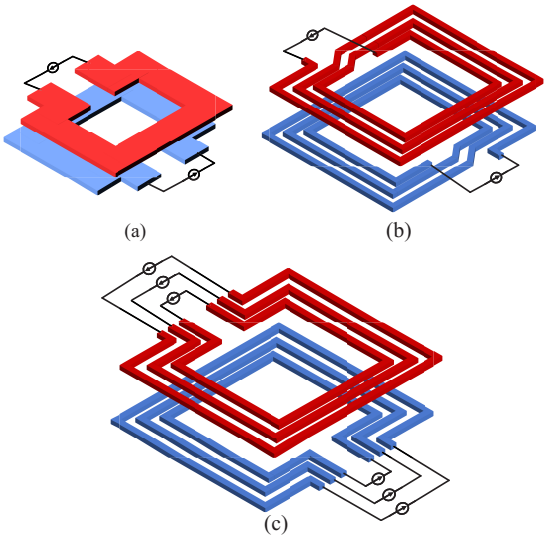

Fig. 1. Illustration of planar-spiral air-core transformer configurations. (a) Single-turn with wide traces, (b) Multi-turn with narrow traces, and (c) Multiple (parallel) windings with independently-controlled (ballasted) currents.

We investigate alternatives where *wide traces are split into narrow traces* to mitigate eddy current effects, or *multi-turn transformer windings are separated into multiple parallel windings*, each with fewer turns, to optimize current distribution. Leveraging passive or active current ballasting [9], [10], we assume the possibility of controlling the current

through each winding independently. As we will show, parallel windings with optimized per-winding current can provide both higher power transfer and higher efficiency.

A central question that arises with the multi-winding transformer is *what is the optimal current to force in each winding? or what is the optimum current density profile to force in the transformer?* These questions are treated using a multi-port impedance matrix for the transformer structure, such as can be extracted from finite-element electromagnetic simulation. The result of the analytical model describes both the amplitude and phase relationships of primary and secondary winding currents that achieve maximum efficiency and maximum power transfer. The result of the analysis is both powerful and general. It can be used to determine the optimal current flow in a wide variety of multi-winding transformers based on a simple impedance-matrix characterization. While this paper doesn't describe 'how' to enforce the per-winding currents, other related works discuss methods to achieve this via impedance-based current ballasting. However, knowledge of the optimal current flow and current-density profile in transformers provides significant design insight and helps to improve efficiency and power-density.

II. Optimal Current Distribution for Multi-Winding Transformers

A multi-winding transformer with multiple primary secondary windings may be modelled as a multi-port network which has a symmetric impedance matrix with N^2 terms, where N is the total number of windings including primary and secondary windings. While Fig. 2 shows an example with multiple single-turn spiral windings, the analysis applies regardless of the number of turns or configuration of the windings. Our analysis does not directly depend on the number of turns in each winding and we use N for the number of windings rather than the number of turns; specifically N_p is the number of primary windings and N_s is the number of secondary windings.

For a general multi-winding transformer of this form, the impedance matrix may be compactly written as

$$\boldsymbol{Z} = \begin{bmatrix} \boldsymbol{R_p} + j\boldsymbol{X_p} & \boldsymbol{R_m} + j\boldsymbol{X_m} \\ (\boldsymbol{R_m} + j\boldsymbol{X_m})^T & \boldsymbol{R_s} + j\boldsymbol{X_s} \end{bmatrix}, \tag{1}$$

where $\boldsymbol{R_p}$ and $\boldsymbol{R_s}$ are the resistance matrices of the primary and secondary sides respectively. $\boldsymbol{X_p} = \omega \boldsymbol{L_p}$ and $\boldsymbol{X_s} = \omega \boldsymbol{L_s}$ are the reactance due the primary and secondary inductance matrices, $\boldsymbol{L_p}$ and $\boldsymbol{L_s}$. $\boldsymbol{R_m}$ is the mutual resistance matrix and $\boldsymbol{X_m} = \omega \boldsymbol{L_m}$ is the reactance of the mutual inductance matrix, $\boldsymbol{L_m}$, which links the primary and secondary windings.

As shown in (Fig. 2) the analytical treatment presumes N_p and N_s sinusoidal currents driving each winding of the primary and secondary sides respectively. Current and voltage polarities in Fig. 2 are defined such that *power flowing into the transformer is positive* while *power flowing out is negative*. We presume all currents are at the same frequency, but their

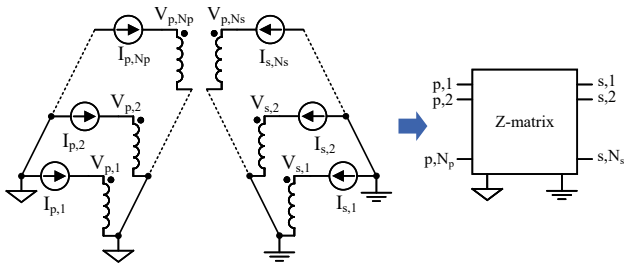

Fig. 2. Multi-port model of a multi-winding transformer.

individual amplitudes and phases may be independently chosen to maximize power efficiency.

Given the desired objective, we first define our notation. The k^{th} input current of the primary side is denoted as $I_{p,k} = \hat{I}_{p,k} e^{j\theta_{p,k}}$, where $\hat{I}_{p,k}$ and $\theta_{p,k}$ are its amplitude and phase respectively with $k \in [1, ..., N_p]$. Similarly, the n^{th} secondary side output current ($n \in [1, ..., N_s]$) is denoted as, $I_{s,n} = \hat{I}_{s,n} e^{j\theta_{s,n}}$ with amplitude, $\hat{I}_{s,n}$ and phase, $\theta_{s,n}$. Hence, we are presented with an optimization problem over $(N_p + N_s)$ complex-variables.

Since we are trying to maximize efficiency, its mathematical expression will serve as the cost function for this optimization. To construct the efficiency function, we first analyze the per-winding *real* power. This approach, as we shall see soon, provides an intuitive understanding of the trade-offs involved without compromising the mathematical rigor. From network theory we can compute real power dissipated (consumed) by an individual primary (secondary) branch as,

$$P_{real} = \mathrm{Re}\left(V \cdot I^*\right)/2$$

where, V is any branch voltage and I^* is the complex conjugate of the branch current in a network.

While the interested reader may consult Appendix A for the full derivations, the key expressions are as follows. The total real power supplied by all the primary side input current sources is given by

$$P_P = P_{P,self} + P_{PS} + P_M \tag{2}$$

where $P_{P,self}$ captures power loss due to primary-side current conduction, associated with resistance matrix $\boldsymbol{R_p}$. P_{PS} captures real power transmitted (received) by the primary (secondary). Finally, P_M includes power associated with the mutual resistance matrix $\boldsymbol{R_m}$, which captures transresistive interactions between the primary and secondary (effects which are typically small in modestly coupled transformers).

Similar to the primary side calculation, the secondary calculation proceeds as,

$$P_S = P_{S,self} - P_{PS} + P_M \tag{3}$$

where $P_{S,self}$ captures the conduction losses due to the resistances in $\boldsymbol{R_s}$ of the secondary side.

Presuming that the primary side is supplying power and the secondary side is receiving power, using the polarities defined in Fig. 2, combined with (2) and (3), efficiency goes as,

$$\eta = -\frac{P_S}{P_P} = \frac{P_{PS} - P_M - P_{S,self}}{P_{PS} + P_M + P_{P,self}}. \quad (4)$$

As mentioned above, in scenarios with moderate to weak coupling between the primary and secondary, such as are common in wireless power transfer and air-core-based isolated power transfer, mutual resistances in $\boldsymbol{R_m}$ may be two or three orders of magnitude lower than resistances in $\boldsymbol{R_p}$ and $\boldsymbol{R_s}$. In this paper going forward, we will neglect $\boldsymbol{R_m}$ terms and assume $P_M = 0$ to simplify the analysis and make general intuitive conclusions without significant loss of accuracy.

A. Optimal Phase Relationships Among Transformer Windings

With the assumption that mutual resistance terms P_M are negligible in (4), trigonometric relationships can be used to show that efficiency is maximized when:

$$\theta_{p,k} = \theta_p \quad (5)$$

$\forall\ k$, where θ_p is a constant.

$$\theta_{s,n} = \theta_s \quad (6)$$

$\forall\ n$, where θ_s is a constant. Finally,

$$\theta_p - \theta_s = \pi/2. \quad (7)$$

This signifies that for optimal operation, the winding currents in the primary side should all have the same phase. The secondary side currents should also have the same phase as each other but should lag the primary currents by 90^o. Such orthogonal phasing for the simplistic case of single winding transformers is well-known and used in wireless power transfer applications [11], [12]. Going ahead, we will set $\theta_p = 0$ as a reference phase and thereby get $\theta_s = -\pi/2$.

B. Optimal Current Amplitudes Among Transformer Windings

The optimal phases can now be substituted in (2) and (3) to obtain significant simplification. Due to phase alignment of the currents in the same side, we need only specify the current amplitudes, which we denote as vectors $\hat{\boldsymbol{I}}_{\boldsymbol{p}} = [\hat{I}_{p,1}, ..., \hat{I}_{p,N_p}]^T$ and $\hat{\boldsymbol{I}}_{\boldsymbol{s}} = [\hat{I}_{s,1}, ..., \hat{I}_{s,N_s}]^T$ for the primary and secondary windings, respectively. Thus, (2) can be shown to be modified to become

$$P_P = \frac{1}{2}\left(\hat{\boldsymbol{I}}_{\boldsymbol{p}}{}^T \boldsymbol{X_m} \hat{\boldsymbol{I}}_{\boldsymbol{s}} + \hat{\boldsymbol{I}}_{\boldsymbol{p}}{}^T \boldsymbol{R_p} \hat{\boldsymbol{I}}_{\boldsymbol{p}}\right), \quad (8)$$

and (3) becomes

$$P_S = \frac{1}{2}\left(\hat{\boldsymbol{I}}_{\boldsymbol{s}}{}^T \boldsymbol{R_s} \hat{\boldsymbol{I}}_{\boldsymbol{s}} - \hat{\boldsymbol{I}}_{\boldsymbol{p}}{}^T \boldsymbol{X_m} \hat{\boldsymbol{I}}_{\boldsymbol{s}}\right). \quad (9)$$

We use the impedance matrix of the multi-winding transformer (1), to relate to the resistance and reactance matrices used in the above expressions. The term $P_{PS} = \hat{\boldsymbol{I}}_{\boldsymbol{p}}{}^T \boldsymbol{X_m} \hat{\boldsymbol{I}}_{\boldsymbol{s}}$ is the transmitted power from the primary to the secondary side under optimal phase conditions. Using (8) and (9), we can also compute the overall conduction loss in the multi-winding transformer,

$$P_{loss} = P_P + P_S = \frac{1}{2}\left(\hat{\boldsymbol{I}}_{\boldsymbol{p}}{}^T \boldsymbol{R_p} \hat{\boldsymbol{I}}_{\boldsymbol{p}} + \hat{\boldsymbol{I}}_{\boldsymbol{s}}{}^T \boldsymbol{R_s} \hat{\boldsymbol{I}}_{\boldsymbol{s}}\right). \quad (10)$$

We may now perform standard convex optimization to maximize the efficiency function, $\eta = -\frac{P_S}{P_P}$. The result obtained is a system of matrix equations given by

$$\left(\frac{P_{loss}^2}{4 P_P P_S}\right) \hat{\boldsymbol{I}}_{\boldsymbol{p}} = \lambda_{com} \hat{\boldsymbol{I}}_{\boldsymbol{p}} = \boldsymbol{M_p} \hat{\boldsymbol{I}}_{\boldsymbol{p}}, \quad (11)$$

for the primary side and similarly for the secondary side,

$$\lambda_{com} \hat{\boldsymbol{I}}_{\boldsymbol{s}} = \boldsymbol{M_s} \hat{\boldsymbol{I}}_{\boldsymbol{s}}. \quad (12)$$

We denote $\boldsymbol{M_p} = (\boldsymbol{X_m^T})^+ \boldsymbol{R_s} \boldsymbol{X_m^+} \boldsymbol{R_p}$ and $\boldsymbol{M_s} = \boldsymbol{X_m^+} \boldsymbol{R_p} (\boldsymbol{X_m^T})^+ \boldsymbol{R_s}$. $(\boldsymbol{X_m^T})^+$ and $\boldsymbol{X_m^+}$ are the pseudo-inverses of $\boldsymbol{X_m}^T$ and $\boldsymbol{X_m}$, respectively. We observe that (11) and (12) are of the form $\lambda \boldsymbol{v} = \boldsymbol{A v}$, where λ and $\boldsymbol{v}$ are the eigenvalues and eigenvectors of the matrix $\boldsymbol{A}$. Thus, we may conclude that, if for $\boldsymbol{M_p}$ and $\boldsymbol{M_s}$ there exists a common eigenvalue λ_{com}, then the solution of the optimal current amplitudes for primary and secondary sides are the eigenvectors of $\boldsymbol{M_p}$ and $\boldsymbol{M_s}$ respectively. We should note that the two eigenvectors only inform us how the primary or secondary currents scale with respect to each other and does not directly tell us the relative scaling between primary and secondary currents.

At this juncture, a question may arise, *which eigenvalue should be chosen if there are multiple common eigenvalues for $\boldsymbol{M_p}$ and $\boldsymbol{M_s}$?* Observing (11), we may show $\lambda_{com} = (1-\eta)^2/4\eta$. This indicates that the closer the efficiency is to unity, the smaller will be λ_{com}. Therefore, we should choose the minimum of all the common eigenvalues. In addition, the relationship between the efficiency and λ_{com} helps us obtain the maximum efficiency as

$$\eta_{max} = (1 + 2\lambda_{com}) - \sqrt{(1+2\lambda_{com})^2 - 1}. \quad (13)$$

This leads to an important conclusion that, for a given multi-winding transformer, there is an intrinsic efficiency maximum determined solely by the impedance matrix $\boldsymbol{Z}$. It is straightforward to show that, in the case of two-winding transformers (a single primary winding and a single secondary winding), the result (13) exactly matches the results previously obtained in the literature [2].

In Appendix B, the relative scaling of primary to secondary current is also derived. The key takeaway, however, is that if we choose the amplitude of $\hat{I}_{s,1} = 1$ as the reference, the value of $\hat{I}_{p,1}$ is scaled by a factor α_{ps}. This, in conjunction with the eigenvectors of $\boldsymbol{M_p}$ and $\boldsymbol{M_s}$, provides optimal current amplitudes for all windings on both sides.

We should take note of the specific yet common case of symmetric multi-winding transformers *i.e.,* identical primary and secondary windings. Here, $\boldsymbol{M_p} = \boldsymbol{M_s}$, and they will share identical eigenvalues and eigenvectors.

Another key point to observe is the form of $\boldsymbol{M_p}$ and $\boldsymbol{M_s}$. As these include the ratio of self-resistances to mutual reactances of the transformer, they capture information on damping or (inverse) quality factor Q. Thus, $\boldsymbol{M_p}$ and $\boldsymbol{M_s}$ provide information on the quality of power transmission (or reception) of a transformer. The closer these matrices are to singular matrices, the higher is the *transmission* Q of the

transformer. Furthermore, this would lead to $\lambda_{com} \to 0$, which means higher efficiency. It should be noted here that efficiency is the combined effect of the transmission efficiency, *i.e.,* how much of the input power is transmitted and reception efficiency, *i.e.,* how much of the transmitted power is finally realized at the output.

In summary, any multi-winding transformer has an intrinsic η_{max} associated with it, which is determined by its impedance matrix $\boldsymbol{Z}$. In typical scenarios (with negligible mutual resistance), to achieve η_{max}, each winding current on a given side (primary or secondary) should have the same phase. The side that is receiving power (secondary) should have current that lags by the transmitting side (primary) by 90^o. Importantly, the impedance matrix $\boldsymbol{Z}$ (which can be determined from FEM simulation or experimental measurement of a transformer) contains sufficient information to determine the optimal excitation amplitudes quickly and accurately.

III. Verification using Numerical Techniques

The analytical results in Section II were verified using numerical optimization in MATLAB using the following procedure:

1) The impedance matrix $\boldsymbol{Z}$ of a sample transformer was obtained from FEM simulations.
2) The *fmincon* optimizer was deployed with $\boldsymbol{Z}$ as its input.
3) We denoted the voltage on primary and secondary windings as $\boldsymbol{V_p}$ and $\boldsymbol{V_s}$ respectively assuming complex primary and secondary current vectors $\boldsymbol{I_p}$ and $\boldsymbol{I_s}$ respectively.
4) The efficiency function was defined as $-P_S/P_P = -\frac{real(\boldsymbol{V_s}\cdot\boldsymbol{I_s^\star})}{real(\boldsymbol{V_p}\cdot\boldsymbol{I_p^\star})}$.
5) We set first secondary winding current amplitude, $I_{s,1}$, to be 1 A and first primary current phase to be $\angle 0^\circ$. The optimizer outputs are the optimal amplitude and phase in all the other N_p+N_s-1 windings to maximize efficiency given the constraint that $P_P > -P_S > 0$.

Results are shown in Fig. 3 to demonstrate the phase alignment on 27 symmetric circular spiral transformer designs with different inner radius and 2, 3, or 4 windings. Consistent with the analysis, Fig. 3 shows that the primary currents phases are close to $\angle 0^\circ$, while those of the secondary side close to $\angle -90^\circ$.

To verify the current distribution, nine symmetric circular spiral transformer designs with different areas were examined. The inner radius, individual trace width and trace-to-trace spacing are kept constant. The designs differ by varying the number of windings from 10 to 60. Consequently, the transformer area also varies. The maximum normalized current distribution difference, defined as $\max(|\hat{I}_{ana,i} - \hat{I}_{num,i}|)$, is less than 0.1% for all the 9 designs. $\hat{I}_{ana,i}$ and $\hat{I}_{num,i}$ represents the i^{th} current for a given design obtained from the analytical calculation and numerical optimization respectively. The difference can be reduced with a tighter tolerance setting in the numerical optimization. Our conclusion is that the difference between the analytical and numerical results is mainly because of the finite accuracy of the numerical method.

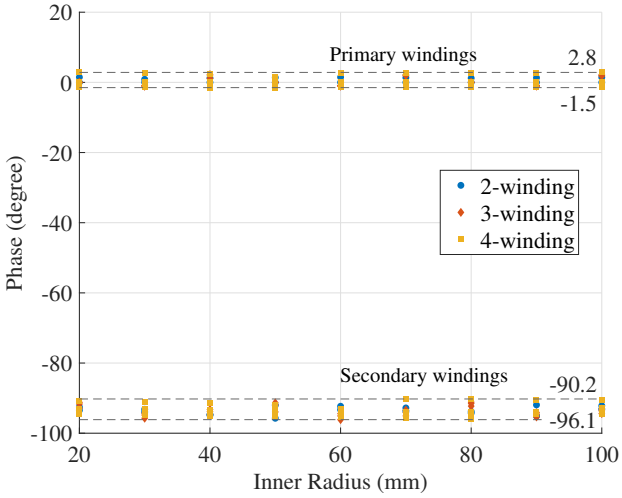

Fig. 3. Numerical optimization results: primary and secondary current phases chosen by the optimizer to maximize efficiency.

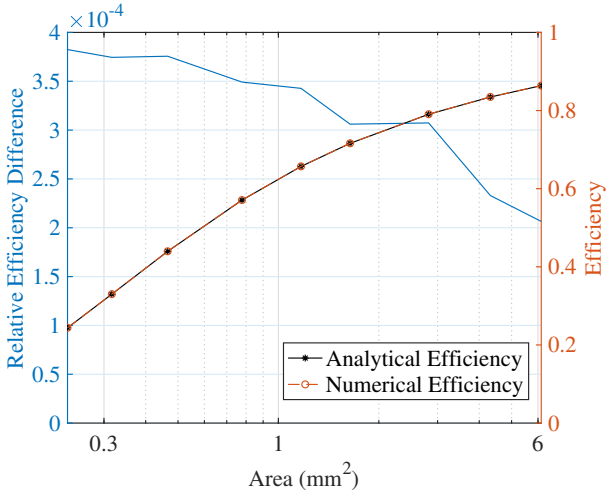

Fig. 4. Efficiency from numerical optimization vs analytical optimal solution. The relative efficiency difference is defined as $(\eta_{num} - \eta_{ana})/\eta_{ana}$.

An alternate verification method performed here is to find the best operation regime with the highest efficiency independently using the numerical and analytical methods. Fig. 4 shows the efficiency obtained from both methods. Across all of the 9 designs, the efficiency difference is less than 0.05%. This further confirms that both the analytical and numerical methods are converging to effectively the same design.

In conclusion, both the optimal phase and optimal amplitude strategy proposed in Section II are effective in finding the best operation regime when mutual resistance is negligible. Approaching the problem with numerical techniques will result in the same choice of operating conditions.

IV. Design Example and Model Insights

To explore, exemplify, and provide design insights, we applied the analytical model to a representative high-frequency planar spiral transformer. We based the example on the available metal stackup, dimensions, and dielectrics in a standard CMOS 180-nm integrated circuit (IC) process. The results are for a symmetric air-core transformer of circular geometry with outermost radius of 1 mm. The primary side transformer has 54 concentric 1-turn windings with uniform width. The separation distance between the primary and secondary sides is varied from 10 µm to 1 mm. The transformer is driven in a similar setup as described in Fig. 2.

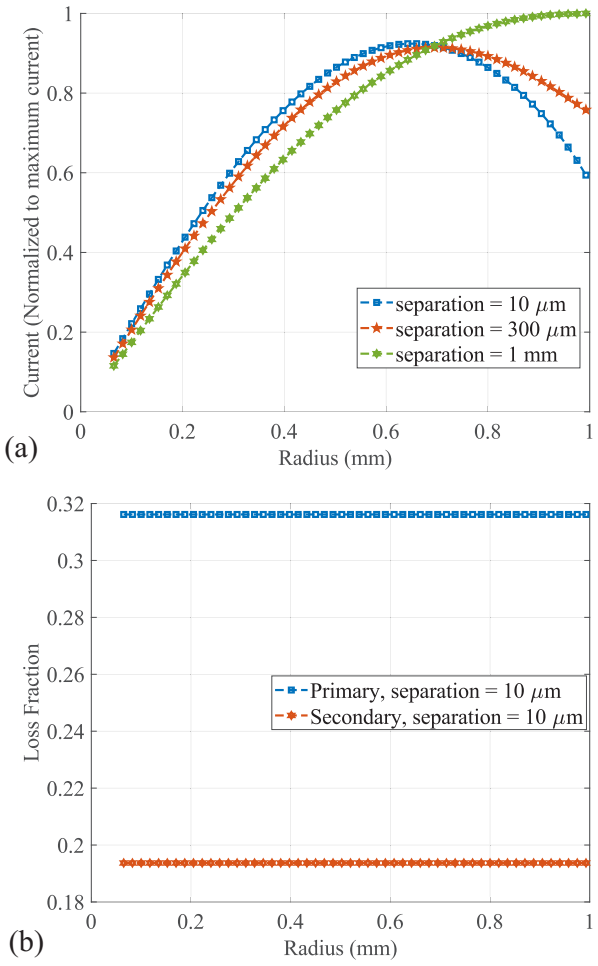

Fig. 5. Optimization results: per winding, by radius (a) primary current distribution profile; (b) Ttransmission and reception loss fraction.

Fig. 5(a) shows an interesting trend regarding the dependence of optimal current distribution on the separation distance between primary and secondary, s. Here the total currents in all cases are the same and the currents are normalized to the maximum winding current across all cases. The winding with the peak current is more centrally located when the separation is small compared to the transformer dimensions. It gradually moves towards the outer radius when the separation becomes larger.

Fig. 5(b) shows the ratio of the power loss to transmitted power in the primary side as well as the ratio of the power loss to received power in the secondary-side windings. These loss fractions provides insight about the per-winding transmission and reception efficiencies of the primary and secondary respectively. Interestingly, the optimal conditions are constant across radius.

For any given winding at the primary side, the coupling between it and any secondary side coil is at its maximum when the two windings are the same size. For a given distance between the primary and secondary side windings, the larger the winding, the better the maximum coupling. For small isolation distances (e.g. 10 µm and 300 µm) and for winding diameters much bigger than s, the rate of increase in coupling with diameter is not as great. In this case the windings with slightly smaller size on the primary side have the best overall power transmission to the secondary side, because they have high coupling to the corresponding secondary winding, and they can couple well to windings that are both smaller and larger than their own diameter. This is depicted in Fig. 6. As a result, the optimal distribution puts the highest current in those windings. In contrast, for a design with a large isolation distance (e.g. 1 mm), the smaller sized windings, due to poor coupling, have poor power transfer, and the optimized current distribution exhibits a monotonically increasing profile with radius.

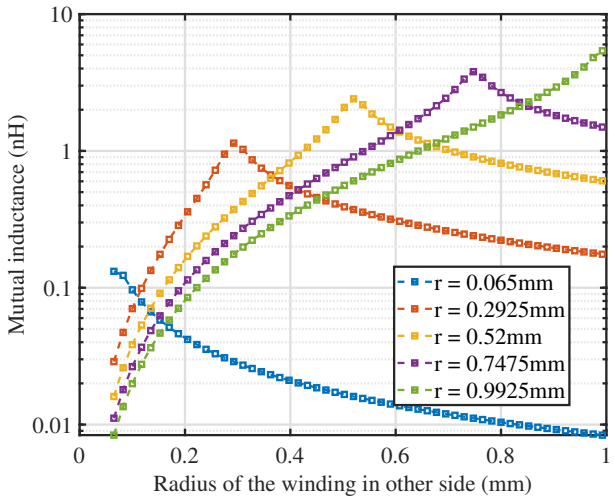

Fig. 6. Mutual inductance of some primary windings with different radius with all secondary windings for $s = 10\mu m$.

Fig. 7 provides a qualitative validation of the above discussion. Here the radial distribution of an estimate of the transmission quality is plotted when the distance of separation is 10 µm. The metric plotted here is defined as the ratio of the total mutual reactive impedance of a particular winding in the primary due to all winding in the secondary side, to the self resistance of that primary side winding. Windings with

radius around 0.7 mm, owing to their superior overall coupling as seen in Fig. 6 and lower resistance than the outermost windings, exhibit the highest transmission Q. Compared to the distribution with the actual radial current distribution in Fig. 5, we find a very strong correlation. This informs us that the optimal distribution is dependent on the transmission quality of the transformer and is maximized in the neighbourhood of the region with the peak transmission Q.

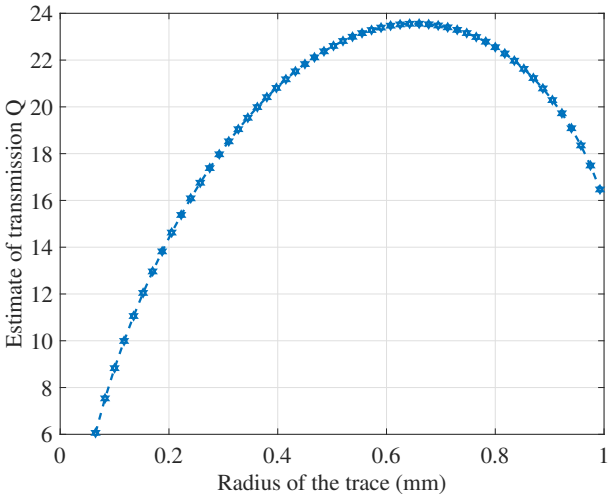

Fig. 7. Radial distribution of approximate transmission quality for $s = 10\mu$m.

V. Experimental Validation

We performed some experiments to validate the theoretical results obtained in Section II.

A. Experimental setup

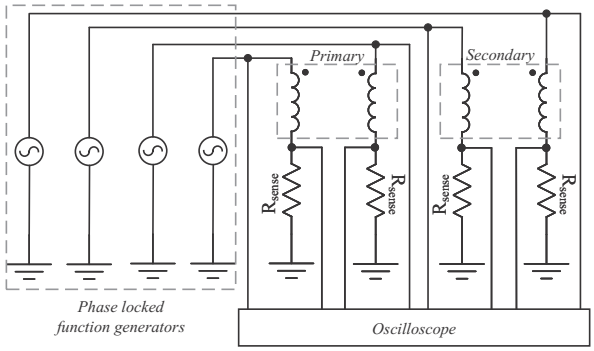

Fig. 8. Schematic of the experimental setup.

The schematic of the setup is shown in Fig. 8. We performed our experiments on a multi-winding transformer with two windings on each of the primary and secondary sides. To establish a challenging scenario for efficient operation, and to make accurate measurement easier, each of the windings has a 1 Ω resistor connected in series. These resistors reduce the Q of the transformer, modifying the overall $\boldsymbol{Z}$. Hence, all comparisons made between the theory and experiments are with this modified $\boldsymbol{Z}$.

Function generators are used to provide sinusoidal excitation at 200 kHz. In order to measure the winding currents they are terminated to ground via series sense resistors. In this experiment, 15 Ω resistance was used. The output of the function generators and the sense resistor voltages are measured using an oscilloscope. The function generators are synchronized in order to ensure correct phase relationships among the currents.

B. Test transformer

The transformer used is shown in Fig. 9. The transformer is constructed using AWG 24 magnet wire wound on a 3D printed circular bobbin. Each of the primary and secondary sides has two windings, one with 10 and one with 15 turns. The transformer impedance matrix is computed using an impedance analyzer [13], [14].

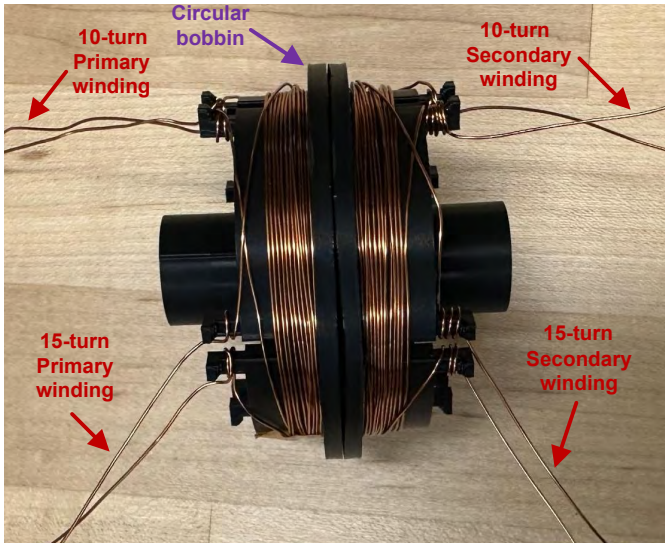

Fig. 9. Wire-wound air-core transformer on a 3D printed circular bobbin.

C. Measurement technique

The validation requires correct measurement of the AC power consumed and delivered at the primary and secondary sides, respectively. As depicted in Fig. 8, the current is obtained by measuring the voltage across the sense resistor and scaling it by the resistance value. The voltage of the winding is measured by taking the difference between the associated function generator and sense resistor voltages. The average value of the product of the measured by winding current and voltage gives the real AC power consumed by the winding.

D. Results

We performed two sets of experiments to compare both single and multi-winding transformer setups. For the single-winding case, we excite one of the two windings on each of the primary and secondary sides of the transformer in Fig.

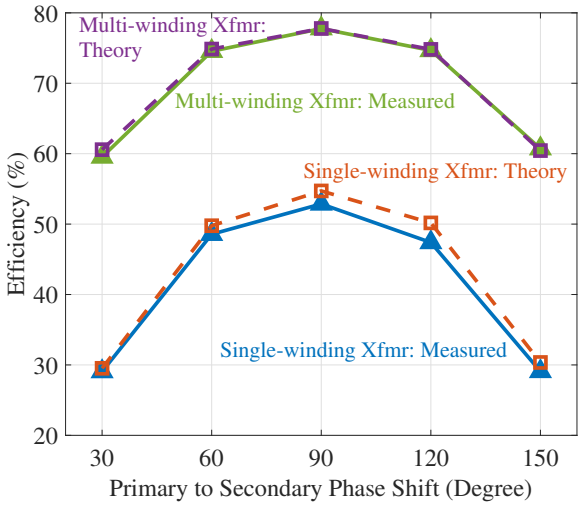

Fig. 10. Measured efficiency.

9. Next, we excite both windings. The excitation amplitudes are adjusted as per the theory and the phase shift between secondary and primary currents is varied. The results obtained are shown in Fig. 10.

In both single- and multi-winding cases, experimental results match very closely with the theoretical calculations. Thus, this provides a good validation of the optimization analysis for multi-winding transformers.

VI. Conclusions

To summarize, this work outlines optimal operating conditions for multi-winding transformers which could be used for wireless or isolated power transfer. An analytical model is developed that can determine the optimal current distribution from the transformer impedance matrix $\boldsymbol{Z}$ which can be derived from FEM simulation or experimental measurement. The model is verified with numerical optimization and can be applied to a wide range of different transformer designs. The results provide insight into winding geometry and operational details. An integrated isolated power converter with this operational regime applied is currently being designed on the basis of the theory. This will provide further confirmation of its accuracy and usefulness.

VII. Acknowledgement

We would like to thank Bob Barry for help with the experimental setup and Conrad Stauth for help with 3D printing the bobbins.

Appendix

A. Efficiency Derivation

We denote any element of the impedance matrix $\boldsymbol{Z}$ as $Z_{p,ab}$, $Z_{s,ab}$ and $Z_{m,ab}$ where, a and b are indices, for primary, secondary or mutual impedances respectively. The complex power on the k^{th} primary winding can be denoted as $S_{p,k} = \frac{1}{2} V_{p,k} \cdot I^*_{p,k}$, which can be expanded as

$$S_P = \frac{1}{2}\sum_{k=1}^{N_p} V_{p,k}\cdot I^*_{p,k} = \frac{1}{2}\left(\sum_{k=1}^{N_p} I_{p,k} Z_{p,kk} I^*_{p,k} + \sum_{a=1}^{N_p}\sum_{b\neq a} I_{p,a} Z_{p,ba} I^*_{p,b} + \sum_{m=1}^{N_p}\sum_{n=1}^{N_s} I_{s,n} Z_{m,mn} I^*_{p,m}\right). \tag{14}$$

Since $Z_{p,ab} = Z_{p,ba}$, (14) can be reorganized as

$$S_P = \frac{1}{2}\left(\sum_{k=1}^{N_p} \hat{I}^2_{p,k} Z_{p,kk} + 2\sum_{a=1}^{N_p-1}\sum_{b=a+1}^{N_p} \hat{I}_{p,a}\hat{I}_{p,b}\cos(\theta_{p,a} - \theta_{p,b}) Z_{p,ab} + \sum_{m=1}^{N_p}\sum_{n=1}^{N_s} I_{s,n} Z_{m,mn} I^*_{p,m}\right). \tag{15}$$

Hence, the real power supplied at the primary side P_P can be expressed as

$$\begin{aligned} P_P = \mathrm{Re}(S_P) = \frac{1}{2}\Bigg(&\sum_{k=1}^{N_p} \hat{I}^2_{p,k} R_{p,kk} \\ &+2\sum_{a=1}^{N_p-1}\sum_{b=a+1}^{N_p} \hat{I}_{p,a}\hat{I}_{p,b} R_{p,ab}\cos(\theta_{p,a} - \theta_{p,b}) \\ &+\sum_{m=1}^{N_p}\sum_{n=1}^{N_s} \hat{I}_{p,m}\hat{I}_{s,n} X_{m,mn}\sin(\theta_{p,m} - \theta_{s,n}) \\ &+\sum_{m=1}^{N_p}\sum_{n=1}^{N_s} \hat{I}_{p,m}\hat{I}_{s,n} R_{m,mn}\cos(\theta_{p,m} - \theta_{s,n})\Bigg). \end{aligned} \tag{16}$$

The correlation of (16) to (2) is as follows.

$$\begin{aligned} P_{P,self} = &\frac{1}{2}\sum_{k=1}^{N_p} \hat{I}^2_{p,k} R_{p,kk} \\ &+\sum_{a=1}^{N_p-1}\sum_{b=a+1}^{N_p} \hat{I}_{p,a}\hat{I}_{p,b} R_{p,ab}\cos(\theta_{p,a} - \theta_{p,b}), \end{aligned} \tag{17}$$

$$P_{PS} = \frac{1}{2}\sum_{m=1}^{N_p}\sum_{n=1}^{N_s} \hat{I}_{p,m}\hat{I}_{s,n} X_{m,mn}\sin(\theta_{p,m} - \theta_{s,n}), \tag{18}$$

$$P_M = \frac{1}{2}\sum_{m=1}^{N_p}\sum_{n=1}^{N_s} \hat{I}_{p,m}\hat{I}_{s,n} R_{m,mn}\cos(\theta_{p,m} - \theta_{s,n}). \tag{19}$$

We can perform the exact same derivation for the secondary side to evaluate the terms in (3). The remaining terms in (3) are given as,

$$\begin{aligned} P_{S,self} = &\frac{1}{2}\sum_{k=1}^{N_s} \hat{I}^2_{s,k} R_{s,kk} \\ &+\sum_{a=1}^{N_s-1}\sum_{b=a+1}^{N_s} \hat{I}_{s,a}\hat{I}_{s,b} R_{s,ab}\cos(\theta_{s,a} - \theta_{s,b}). \end{aligned} \tag{20}$$

With the detailed expressions above and assuming that P_M is negligible we can solve for optimal phases using (4). An intuitive way of solving this with basic trigonometry is as follows. The efficiency expression will be maximized when the $\sin(\theta_{s,n} - \theta_{p,m})$ terms becomes unity. This means any arbitrary $\theta_{s,n}$ and $\theta_{p,m}$ are orthogonal to each other. Since the choice of $\theta_{s,n}$ was arbitrary, all $\theta_{s,n}$ should be equal to each other. The same holds true for $\theta_{p,m}$.

With the phase orthogonality, the efficiency expression becomes,

$$\eta = \frac{\sum_{n=1}^{N_s} \hat{I}_{s,n}(\sum_{k=1}^{N_p} \hat{I}_{p,k} X_{m,kn} - \sum_{x=1}^{N_s} \hat{I}_{s,x} R_{s,nx})}{\sum_{k=1}^{N_p} \hat{I}_{p,k}(\sum_{n=1}^{N_s} \hat{I}_{s,n} X_{m,kn} + \sum_{a=1}^{N_p} \hat{I}_{p,a} R_{p,ka})}. \quad (21)$$

We should also notice that (21) is the ratio of the expanded forms of (9) to (8).

Using (21), we can perform convex optimization to maximize η. While for space constraints we do not provide the full derivation, the key steps are as follows.

We choose any arbitrary primary side current, $\hat{I}_{p,b}$. To find its optimal value, we perform $\frac{\partial \eta}{\partial \hat{I}_{p,b}} = 0$. After some algebraic manipulations, we then get,

$$\left(\frac{\hat{\boldsymbol{I}}_{\boldsymbol{p}}{}^T \boldsymbol{R_p} \hat{\boldsymbol{I}}_{\boldsymbol{p}} + \hat{\boldsymbol{I}}_{\boldsymbol{s}}{}^T \boldsymbol{R_s} \hat{\boldsymbol{I}}_{\boldsymbol{s}}}{\hat{\boldsymbol{I}}_{\boldsymbol{s}}{}^T \boldsymbol{R_s} \hat{\boldsymbol{I}}_{\boldsymbol{s}} - \hat{\boldsymbol{I}}_{\boldsymbol{p}}{}^T \boldsymbol{X_m} \hat{\boldsymbol{I}}_{\boldsymbol{s}}} \right) \sum_{n=1}^{N_s} \hat{I}_{s,n} X_{m,bn} = 2 \sum_{k=1}^{N_p} \hat{I}_{p,k} R_{p,bk}. \quad (22)$$

Since the choice of $\hat{I}_{p,b}$ was arbitrary, (22) hold true for all primary windings. Thus, recalling (9) and (10), the condition for all windings can be compactly written in matrix form as,

$$\left(\frac{P_{loss}}{2P_S} \right) \boldsymbol{X_m}{}^T \hat{\boldsymbol{I}}_s = \boldsymbol{R_p} \hat{\boldsymbol{I}}_p. \quad (23)$$

Similarly, for the secondary side, we can derive,

$$\left(\frac{P_{loss}}{2P_P} \right) \boldsymbol{X_m} \hat{\boldsymbol{I}}_p = \boldsymbol{R_s} \hat{\boldsymbol{I}}_s. \quad (24)$$

We can now use (23) to express $\hat{\boldsymbol{I}}_s$ in terms of $\hat{\boldsymbol{I}}_p$. Then performing substitution to (24) gives us,

$$\left(\frac{P_{loss}^2}{4P_P P_S} \right) \hat{\boldsymbol{I}}_p = (\boldsymbol{X_m}^T)^+ \boldsymbol{R_s} \boldsymbol{X_m}^+ \boldsymbol{R_p} \hat{\boldsymbol{I}}_p. \quad (25)$$

This is exactly (11) in its expanded form. Thus, the optimal primary current scaling is obtained. The secondary currents can derived in the same process starting by eliminating $\hat{\boldsymbol{I}}_p$ to obtain (12).

B. Current Scaling Derivation

Since $\boldsymbol{I_p}$ and $\boldsymbol{I_s}$ are eigenvectors, the relative scaling between the currents will be fixed. We can choose the first current amplitude for both primary and secondary side to be the reference. From it, we obtain

$$\hat{\boldsymbol{I}}_{\boldsymbol{p}} = \hat{I}_{p,1} \begin{bmatrix} 1 & \alpha_{p,2} & \cdots & \alpha_{p,N_p} \end{bmatrix}^T = \hat{I}_{p,1} \boldsymbol{\alpha_p}^T \quad (26)$$

$$\hat{\boldsymbol{I}}_{\boldsymbol{s}} = \hat{I}_{s,1} \begin{bmatrix} 1 & \alpha_{s,2} & \cdots & \alpha_{s,N_s} \end{bmatrix}^T = \hat{I}_{s,1} \boldsymbol{\alpha_s}^T. \quad (27)$$

Plugging (26) and (27) into (8) and (9), we can express the efficiency as

$$\eta = -\frac{P_S}{P_P} = \frac{\hat{I}_{p,1} \hat{I}_{s,1} \boldsymbol{\alpha_p}^T \boldsymbol{X_m} \boldsymbol{\alpha_s} - \hat{I}_{s,1}^2 \boldsymbol{\alpha_s}^T \boldsymbol{R_s} \boldsymbol{\alpha_s}}{\hat{I}_{p,1} \hat{I}_{s,1} \boldsymbol{\alpha_p}^T \boldsymbol{X_m} \boldsymbol{\alpha_s} + \hat{I}_{p,1}^2 \boldsymbol{\alpha_p}^T \boldsymbol{R_p} \boldsymbol{\alpha_p}}. \quad (28)$$

We denote $\hat{I}_{p,1}/\hat{I}_{s,1}$ as α_{ps} Eq. (28) can be reorganized as

$$\eta = \frac{\alpha_{ps} \boldsymbol{\alpha_p}^T \boldsymbol{X_m} \boldsymbol{\alpha_s} - \boldsymbol{\alpha_s}^T \boldsymbol{R_s} \boldsymbol{\alpha_s}}{\alpha_{ps} \boldsymbol{\alpha_p}^T \boldsymbol{X_m} \boldsymbol{\alpha_s} + \alpha_{ps}^2 \boldsymbol{\alpha_p}^T \boldsymbol{R_p} \boldsymbol{\alpha_p}}. \quad (29)$$

As we can obtain the efficiency η from (13), and $\boldsymbol{\alpha_p}^T \boldsymbol{X_m} \boldsymbol{\alpha_s}, \boldsymbol{\alpha_p}^T \boldsymbol{R_p} \boldsymbol{\alpha_p}, \boldsymbol{\alpha_s}^T \boldsymbol{R_s} \boldsymbol{\alpha_s}$ are all known scalars, the valid root of the above quadratic equation may be chosen to obtain the current scaling factor α_{ps}.

REFERENCES

[1] B. Chen, "Fully integrated isolated dc-dc converter using micro-transformers," in *2008 Twenty-Third Annual IEEE Applied Power Electronics Conference and Exposition*, 2008, pp. 335–338.

[2] C. C. Mi, G. Buja, S. Y. Choi, and C. T. Rim, "Modern advances in wireless power transfer systems for roadway powered electric vehicles," *IEEE Transactions on Industrial Electronics*, vol. 63, no. 10, pp. 6533–6545, 2016.

[3] S. Y. R. Hui, W. Zhong, and C. K. Lee, "A critical review of recent progress in mid-range wireless power transfer," *IEEE Transactions on Power Electronics*, vol. 29, no. 9, pp. 4500–4511, 2014.

[4] D. J. Perreault and et. al., "Opportunities and Challenges in Very High Frequency Power Conversion," in *2009 Twenty-Fourth Annual IEEE Applied Power Electronics Conference and Exposition*, Feb. 2009, pp. 1–14.

[5] C. R. Sullivan, B. A. Reese, A. L. F. Stein, and P. A. Kyaw, "On size and magnetics: Why small efficient power inductors are rare," in *2016 International Symposium on 3D Power Electronics Integration and Manufacturing (3D-PEIM)*, Jun. 2016, pp. 1–23.

[6] P. H. McLaughlin, Z. Xia, and J. T. Stauth, "A monolithic resonant switched-capacitor voltage regulator with dual-phase merged-lc resonator," *IEEE Journal of Solid-State Circuits*, vol. 55, no. 12, pp. 3179–3188, 2020.

[7] K. Datta, P. H. McLaughlin, and J. T. Stauth, "A fully-integrated direct-conversion resonant switched capacitor converter with modular multi-winding current ballasting," in *2023 IEEE Custom Integrated Circuits Conference (CICC)*, 2023, pp. 1–2.

[8] P. H. McLaughlin, P. A. Kyaw, M. H. Kiani, C. R. Sullivan, and J. T. Stauth, "A 48-v:16-v, 180-w resonant switched-capacitor converter with high-q merged multiphase lc resonator," *IEEE Journal of Emerging and Selected Topics in Power Electronics*, vol. 8, no. 3, pp. 2255–2267, 2020.

[9] P. H. McLaughlin, Z. Xia, and J. T. Stauth, "11.2 a fully integrated resonant switched-capacitor converter with 85.5% efficiency at 0.47w using on-chip dual-phase merged-lc resonator," in *2020 IEEE International Solid-State Circuits Conference - (ISSCC)*, 2020, pp. 192–194.

[10] P. A. Kyaw, A. L. F. Stein, and C. R. Sullivan, "High-q resonator with integrated capacitance for resonant power conversion," in *2017 IEEE Applied Power Electronics Conference and Exposition (APEC)*, 2017, pp. 2519–2526.

[11] S. Li and C. C. Mi, "Wireless power transfer for electric vehicle applications," *IEEE Journal of Emerging and Selected Topics in Power Electronics*, vol. 3, no. 1, pp. 4–17, 2015.

[12] T. Yilmaz, N. Hasan, R. Zane, and Z. Pantic, "Multi-objective optimization of circular magnetic couplers for wireless power transfer applications," *IEEE Transactions on Magnetics*, vol. 53, no. 8, pp. 1–12, 2017.

[13] S. Prabhakaran and C. Sullivan, "Impedance-analyzer measurements of high-frequency power passives: techniques for high power and low impedance," in *Conference Record of the 2002 IEEE Industry Applications Conference. 37th IAS Annual Meeting (Cat. No.02CH37344)*, vol. 2, 2002, pp. 1360–1367 vol.2.

[14] Y. Wu and C. R. Sullivan, "Performance comparison of miniaturized isolation transformer topologies," in *2023 IEEE Applied Power Electronics Conference and Exposition (APEC)*, 2023, pp. 2654–2660.